Incremental Damage Model for Fatigue Life Assessment in Complete Machinery Simulation

Marcus Lilja, Jesper Karlsson, Anders Jonsson, Daniel Hilding
DYNAmore Nordic AB
Stefan B. Lindström, Daniel Leidermark, Peter Schmidt
Division of Solid Mechanics, Linköping University

Abstract

In CAE today a transition towards "complete machinery simulation", away from the traditional component or sub-assembly simulation, is seen. The complete, assembled and pre-loaded machine is simulated with real loads and boundary conditions which minimizes the risk of errors in the boundary conditions and loading. The longer simulation time is mitigated by the reduction in the number of load cases needed and that a single simulation yields the results for all components. This "complete machinery simulation"-approach is not new, e.g. in the automotive industry LS-DYNA® has been used for realistic simulations for many years and this approach has now reached other industry sectors as well. When developing e.g. heavy industrial equipment, static strength is not a common failure mode, but fatigue is. Fatigue life estimation of a product is crucial and since fatigue tests are both expensive and time-consuming there is a need for accurate fatigue simulation methods.

Fatigue analysis within the CAE-process is commonly based on the rainflow count method for cycle counting and the Palmgren-Miner's linear damage accumulation model. The fatigue life prediction is performed on the result history from a previous analysis and is dependent on the output frequency so that all peaks and valleys of the result variation are identified. This method is widely used and is well-suited for most of the common fatigue scenarios today. However, when using complete machinery simulation, shortcomings in the above method have been identified to be caused by the combination of very large models, high frequency output, and non-proportional loading. This tends to result in a great amount of data for the subsequent fatigue analysis. The amount of data makes post processing and fatigue analysis cumbersome and since development is an iterative process, disk space may become a critical factor.

This paper presents an implementation of the incremental fatigue model of Ottosen and co-workers [Int. J. Fatigue, 30:996-1006 (2008)] as a user-material for LS-DYNA. The model offers a uniform framework for multiaxial, non-proportional and non-cyclic loading. With this model, the fatigue assessment is made on the element level during the simulation. The model enhances performance in terms of faster integration, less data storage, and easier usage. A comparison of the fatigue life predicted using the new method to the standard rainflow count method for selected grades of steel and aluminum is presented.

Motivation for a Continuous-Time High Cycle Fatigue Damage Model

When simulations are performed on large and/or complex structures where the structural response is in the high frequency region and high-cycle or giga-cycle fatigue is of interest some issues arises. To increase the accuracy of the results in such a simulation, a large amount of result data is often required, due to the difficulty in determining when and where stress maxima and minima for the fatigue cycle definition will occur. In many cases the hardware resources will be the limiting factor and a decision must be made where accuracy is traded for speed or even the possibility to perform such simulation at all. The fatigue model presented in this paper minimizes the above issues since the fatigue damage is continuously updated, in the time domain, throughout the simulation. The users do not need to extract gigabytes of data for a subsequent fatigue analysis. This increases the efficiency, and potentially the accuracy, when performing fatigue life predictions for complete machinery simulations. This paper shows the early steps taken in developing a Continuous-Time High Cycle Fatigue model, CTHCF, as a user-defined material model for LS-DYNA. Benchmarks of simple examples with results comparison to traditional fatigue life estimation methods are shown and issues with the presented fatigue model are discussed.

Application example: Rock drill.

Due to economics, a rock drill, see Figure 1, must be extremely reliable, since any down time may result in direct loss of income for the customer. The product is designed for heavy-duty operation and product fatigue life is a key issue. In the case of a rock drill fatigue means Ultra High-Cycle Fatigue (or Giga-Cycle Fatigue), i.e. $> 10^9$ cycles to failure.

Figure 1. Rock drilling equipment.

The 'high-end' simulation strategy of today for some companies that develop equipment for the mining industry is Realistic Simulation. This means that the simulation will start with the assembly and pre-loading of the complete machine FE-model, which is then subjected to actual measured loads (or loads from system simulations). The objective of this simulation method is to capture both local and global physics phenomena.

For such simulations, a highly resolved mesh is needed for stress resolution since converged stress values are of importance for fatigue analysis, especially in the giga-cycle regime where a slight difference in stress amplitude or range will have a large effect on the predicted fatigue life. In many cases, simulating the complete machine is not enough. In order to obtain a correct response from the machine FE-model, also the surroundings (attachments, rigs, drill string etc.) must be included in the FE-model to obtain realistic boundary conditions. In the rock-drill case it is necessary to include part of the surrounding supporting structure as well. The stresses will be induced by either the internal pressure pulses, the global structural motion or a combination thereof. So, in the end, the model will have to contain millions of elements for the sake of result accuracy

Traditional fatigue analysis using finite elements is often based on the principle of rain flow count and the Palmgren-Miner rule for damage accumulation. To perform this type of analysis the complete stress history needs to be known, otherwise rain flow counting is not possible.

The problem identified with this method is that for a rock-drill case the amount of accumulated output data will be very large. The rock drill has a broad frequency content in its structural response and millions of elements to output. In cases such as this, the fatigue analysis becomes very time consuming and sometimes it is not even possible to perform the fatigue analysis due to the amount of result data. This has been confirmed by our exercises on applications including, but not limited to, rock-drills. Also, since fatigue analysis are performed as an integrated part of the product development cycle, analysis results from several simulations of different designs must be stored for comparison, which further increases the disk space demand.

In short, it would be preferable for cases such as the rock drill to utilize a fatigue analysis approach without cycle counting, since the fatigue cycle definition and the cycle counting are what requires the great amount of data for accuracy.

Incremental Fatigue Model

The CTHCF-model is described as a Drucker-Prager type surface where the motion of this surface comes from kinematic hardening represented by a back stress. The back stress is also used for memorizing the stress history and the surface is a damage surface instead of a yield surface. This model was first presented by Ottosen et. al. [1] and has then been further investigated and improved by Lindström et. al [2,3].

Governing equations

Consider $\boldsymbol{\sigma}(\mathbf{t})$ to be the time dependent stress evolution in a material point in the fatigue analysis. The fatigue model, initially presented by Ottosen et al. [1], is based on the concept of an endurance surface, Eq. (1) where an endurance function β, Eq. (2), determines if damage is caused or not by the present stress evolution. β is a function of the stress evolution, $\boldsymbol{\sigma}$, and the deviatoric back stress, $\boldsymbol{\alpha}$. The present implementation of the model is limited to fatigue damage in isotropic materials for the time being (anisotropic formulations are also available [4]).

$$\{\boldsymbol{\sigma} : \beta(\boldsymbol{\sigma}, \boldsymbol{\alpha}) = 0\} \tag{1}$$

$$\beta(\boldsymbol{\sigma}, \boldsymbol{\alpha}) = \frac{1}{E}\left[\sigma_{eff}(\boldsymbol{\sigma}, \boldsymbol{\alpha}) + Atr(\boldsymbol{\sigma}) - S_e\right] \tag{2}$$

Above, S_e is the endurance stress, A is a material constant, $tr(\boldsymbol{x})$ denotes the trace of a tensor $\mathbf{x}$ and E is the Young's modulus (used as reference stress only).
The effective stress is based on the deviatoric stress as:

$$\sigma_{eff}(\boldsymbol{\sigma}, \boldsymbol{\alpha}) = \sqrt{\frac{3}{2}}\|\boldsymbol{s} - \boldsymbol{\alpha}\| \tag{3}$$

using the deviator $\boldsymbol{s}$ of the stress and the Frobenius norm ($\|\boldsymbol{x}\| = \sqrt{\boldsymbol{x}:\boldsymbol{x}}$). The above implies that the endurance surface, $\beta = 0$, may be visualized as a cone with its axis intersecting $\boldsymbol{\alpha}$ and being parallel to the hydrostatic line in principal stress space, see Figure 3.

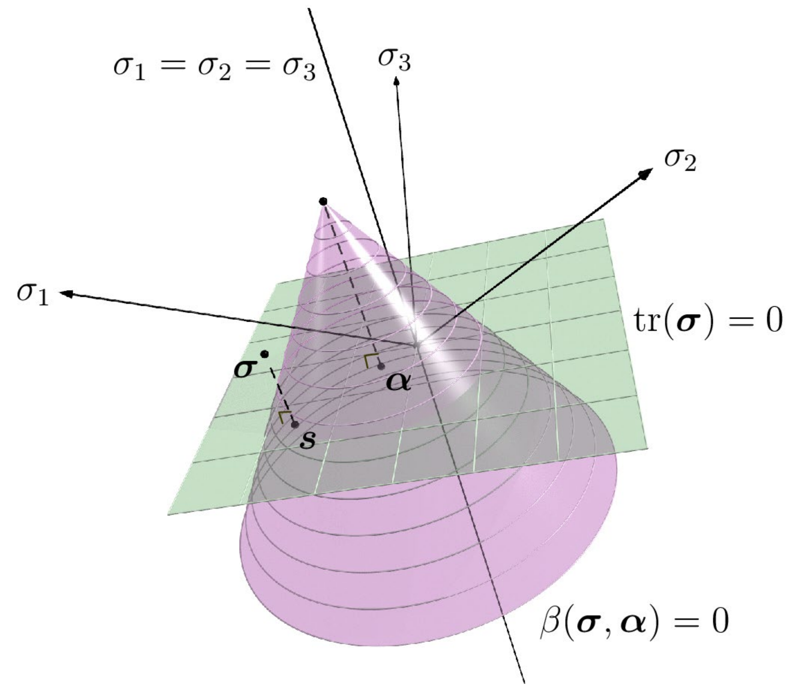

Figure 3. The endurance surface, $\boldsymbol{\beta = 0}$ (cone), and deviatoric plane tr(σ) = 0 in principal stress space.

The fatigue damage

The damage, D, is a scalar ranging from 0 to 1 where D=0 indicates an undamaged material while D=1 indicates critical material fatigue damage. The state variables D and $\boldsymbol{\alpha}$ are defined by the initial value problem shown in eq. 4 and eq. 5.

$$\dot{\boldsymbol{\alpha}} = (\boldsymbol{s} - \boldsymbol{\alpha})\boldsymbol{C}\boldsymbol{H}(\beta)\boldsymbol{H}(\dot{\beta})\dot{\beta} \qquad \boldsymbol{\alpha}(0) = \boldsymbol{0}, \qquad (4)$$

$$\dot{\boldsymbol{D}} = \boldsymbol{g}(\beta)\boldsymbol{H}(\beta)\boldsymbol{H}\big(\dot{\beta}\big)\dot{\beta} \qquad D(0) = 0 \qquad (5)$$

$$\boldsymbol{g}(\beta) = K \cdot e^{L\beta} \qquad (6)$$

where $C, K\ and\ L$ are material constants (>0) and g is a function such that $g(\beta) > 0$ when $\beta > 0$.
Also, H is the Heaviside step function, which means that both $\beta > 0$ and $\dot{\beta} > 0$ is required for damage to develop.

This CTHCF-model contain the five material parameters: S_e, *A, C, K* and *L,* who are determined through material testing and parameter identification.

Properties of the CTHCF-model compared to some existing software

Table 1 highlights some of the differences found when comparing the CTHCF-model to an existing fatigue software. Note that the comments apply to the software used for this comparison, for some existing software this may not be correct.

Table 1. CTHCF versus existing fatigue software

	CTHCF-model	Existing software
Execution	Transient simulation	Post-Processing
Requires S-N-input	No*	Yes
Stress used	Max. Shear	Max. Principal
Multiplane	Any plane	Critical plane
Fatigue limit	Material model-based endurance function	S-N curve
Mean stress effect	Included	Haigh diagram
Output frequency	Optional	Critical

**Needed for parameter fit, not for actual calculation*

The properties shown in Table 1 reveals that the CTHCF-model will be independent on the output frequency (no cycle counting) which will result in much less data to process, which was one of the main objectives. It also considers multiaxial states, and mean stress effects will be treated automatically. The model features many of the properties that are attractive in a Continuous-Time fatigue approach.

Material parameter identification

A material parameter identification is needed to find the parameters necessary for the CTHCF-model. Figure 4 shows fitting results for 7050-T7451 aluminum alloy when different stress ratios were used.

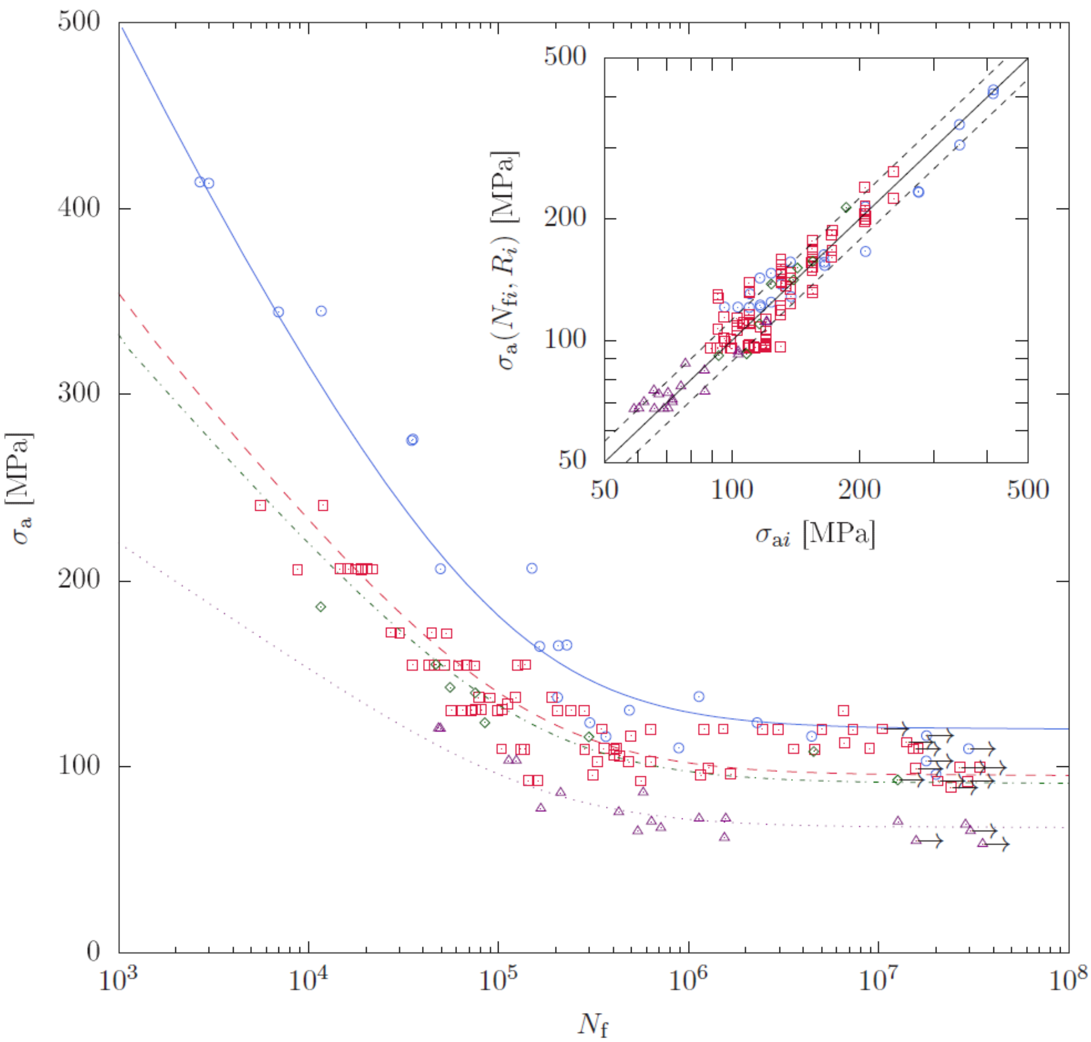

Figure 4. Parameter fit for 7050-T7451 aluminium alloy plate. The lines represent the model fit while the scatter data points are measurement conducted at different stress ratios: R = −1 (circles, solid line), R = 0 (squares, dashed line), R = 0.1 (diamonds, dash-dotted line) and R = 0.5 (triangles, dotted line).

The material parameters for 7050-T7451 aluminium alloy and AISI 4340 steel that were determined in the tests and used in the CTHCF-model are found in Table 2.

Table 2. 7050-T7451 aluminium alloy and AISI 4340 steel material parameters

	E [GPA]	S_E [MPA]	A	C	K	L
7050-T7451	71.7	120.3	0.2608	495.5	0.005117	1550.0
AISI 4340	200.0	492.1	0.2964	718.0	0.020060	1032.0

S-N curve prediction

By running the CTHCF-model to runout using different stress amplitudes it was possible to re-create the S-N curve from the fatigue tests, shown in Figure 4. Figure 5 shows the result for this exercise for 7050-T7451; the agreement is good. This should mean that the CTHCF-model describes the material fatigue properties well for these test conditions.

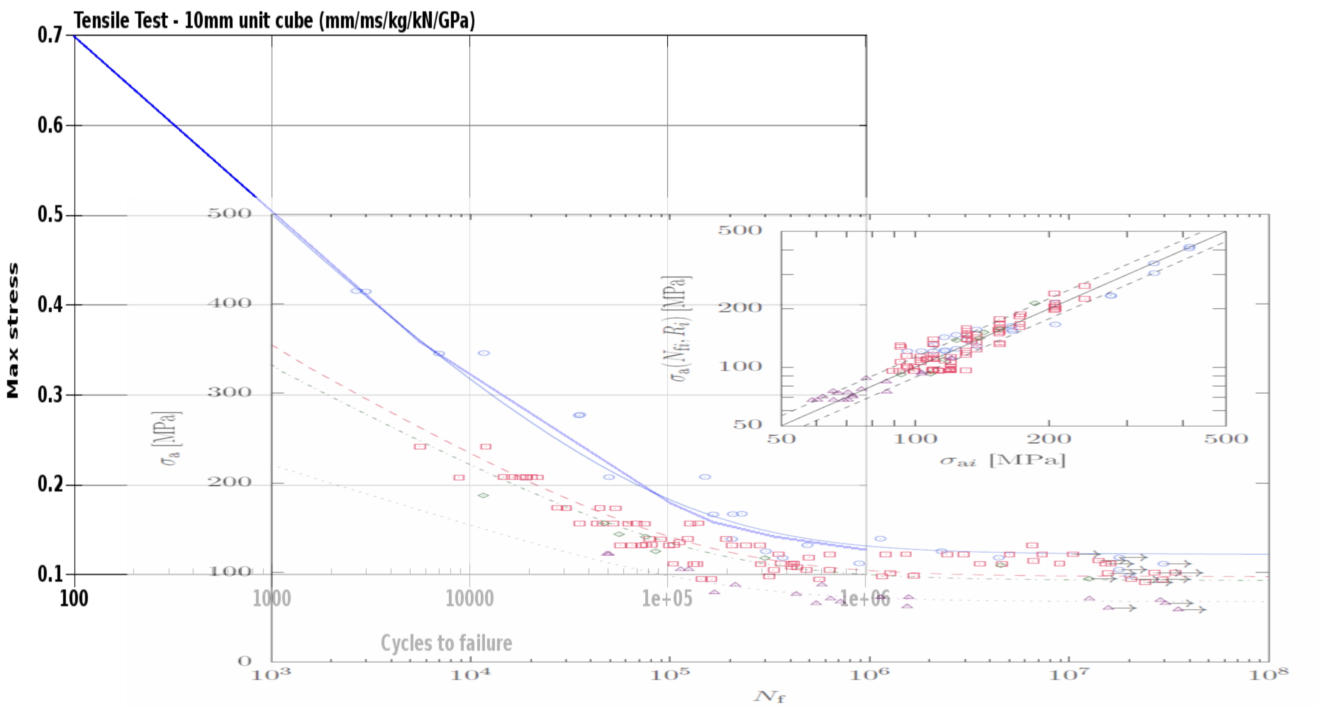

Figure 5. The CTHCF-model vs. fatigue test S-N curve.

Incremental Fatigue Model – Benchmark

The CTHCF-model was benchmarked against the LS-DYNA[8] fatigue solver (using `*FATIGUE_{OPTION}`) and the METApost[7] plug-in fatigue solver mFAT[5][6]. Several simulations were performed including proportional, non-proportional, in-phase and out-of-phase loading of simple models. Also, a check was made to see what solution time penalty, if any, that the CTHCF-model might introduce.

A Simple 1-element model.

The first benchmark was made as simple as possible: a 10 mm cube, see Figure 6 for the model and Figure 7 for the applied boundary conditions. Only one hex element (ELFORM= -1) was used. The material used was 7050-T7451(aluminium alloy)

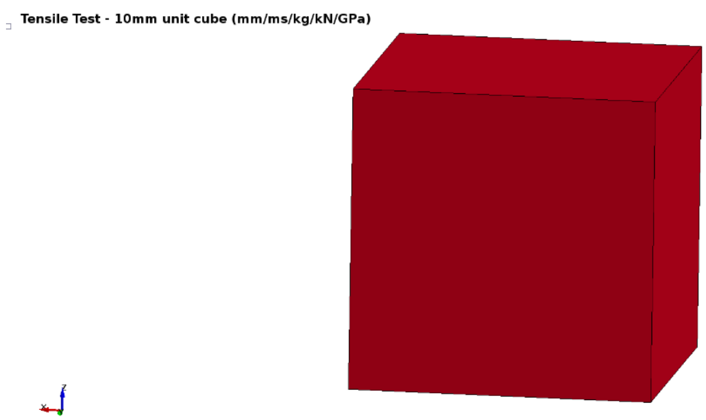

Figure 6. 1-element model.

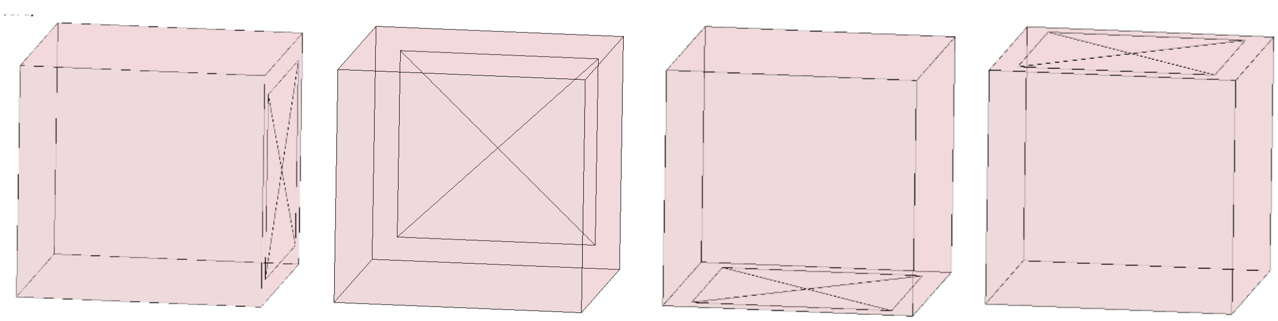

Figure 7. x-, y-, z-constrained motion and area where the z-load is applied.

Uniaxial, proportional loading with a constant amplitude

Applied stress:

$$\sigma_{33} = \sigma_0 \cdot \sin(\omega t), \quad (5a)$$

$$\sigma_{11} = \sigma_{22} = \sigma_{12} = \sigma_{13} = \sigma_{23} = 0 \quad (5b)$$

Figure 8 shows the resulting element stress response, when loading the cube model seen in Figure 6, from a uniaxial and proportional load case. The curves represent the axial stress(green), the shear stress(red) and the von Mises effective stress(blue), respectively.

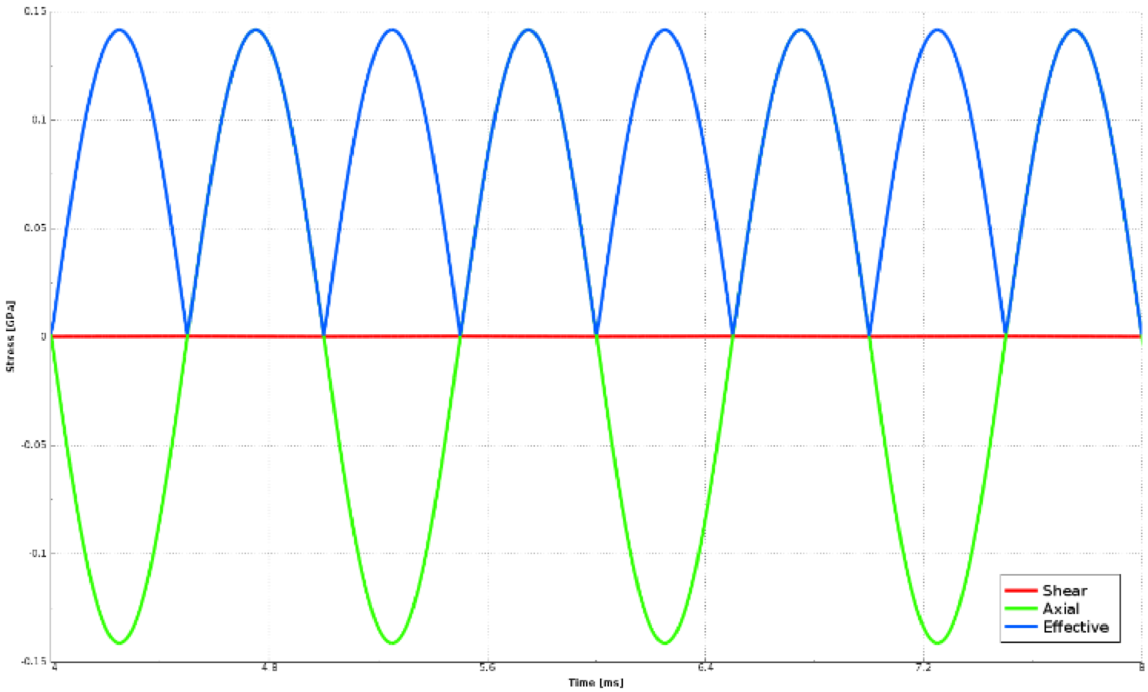

Figure 8. Constant amplitude loading, element stress.

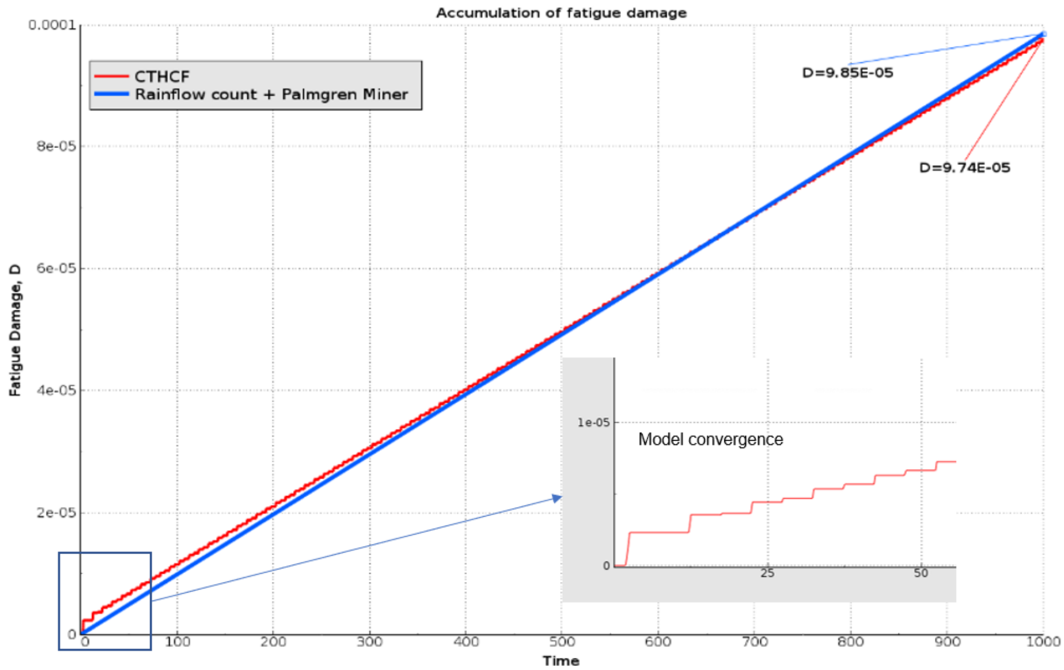

Figure 9. CTHCF compared to RFC+PM, constant amplitude.

The difference in result is about 1% when comparing the CTHCF-model to a more traditional approach for fatigue damage calculation, see Figure 9. The CTHCF-model needed 1-3 cycles to converge, which might be an issue for load spectra containing more varying amplitudes.

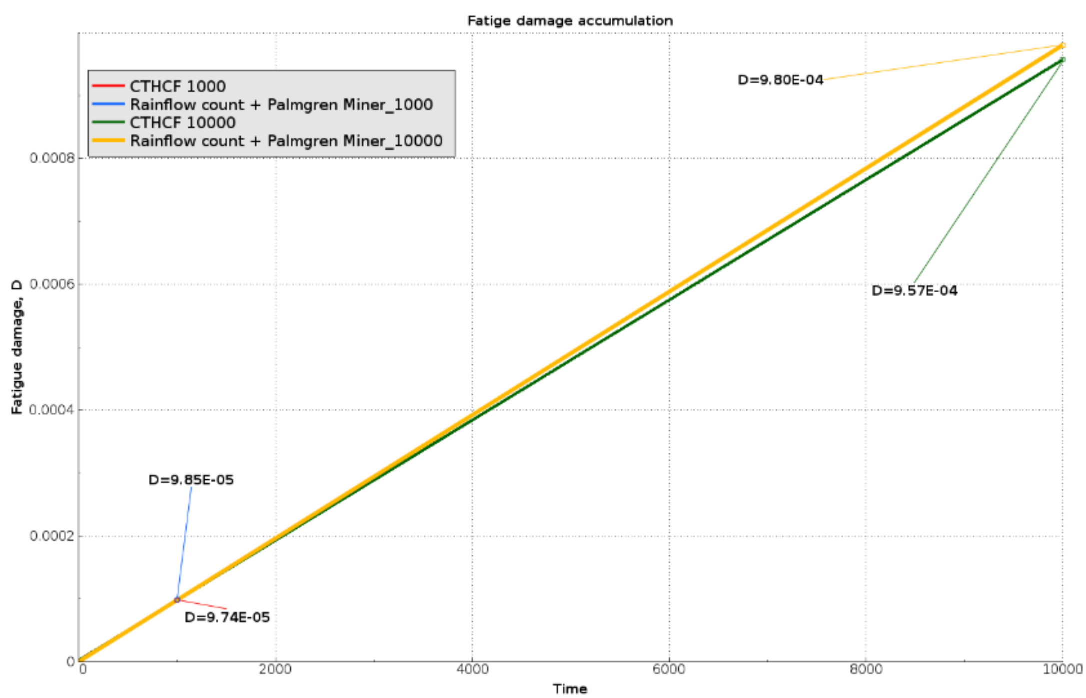

Figure 10. CTHCF compared to RFC+PM for 1000 and 10000 cycles, constant amplitude.

Figure 10 shows that the difference in damage increases from 1% to 2% when the number of cycles is increased from 1000 to 10000.

Uniaxial, proportional loading with a varying amplitude

Comparison between CTHCF and traditional rainflow count + Palmgren Miner for different number of load-peaks in a load spectrum of varying amplitudes.

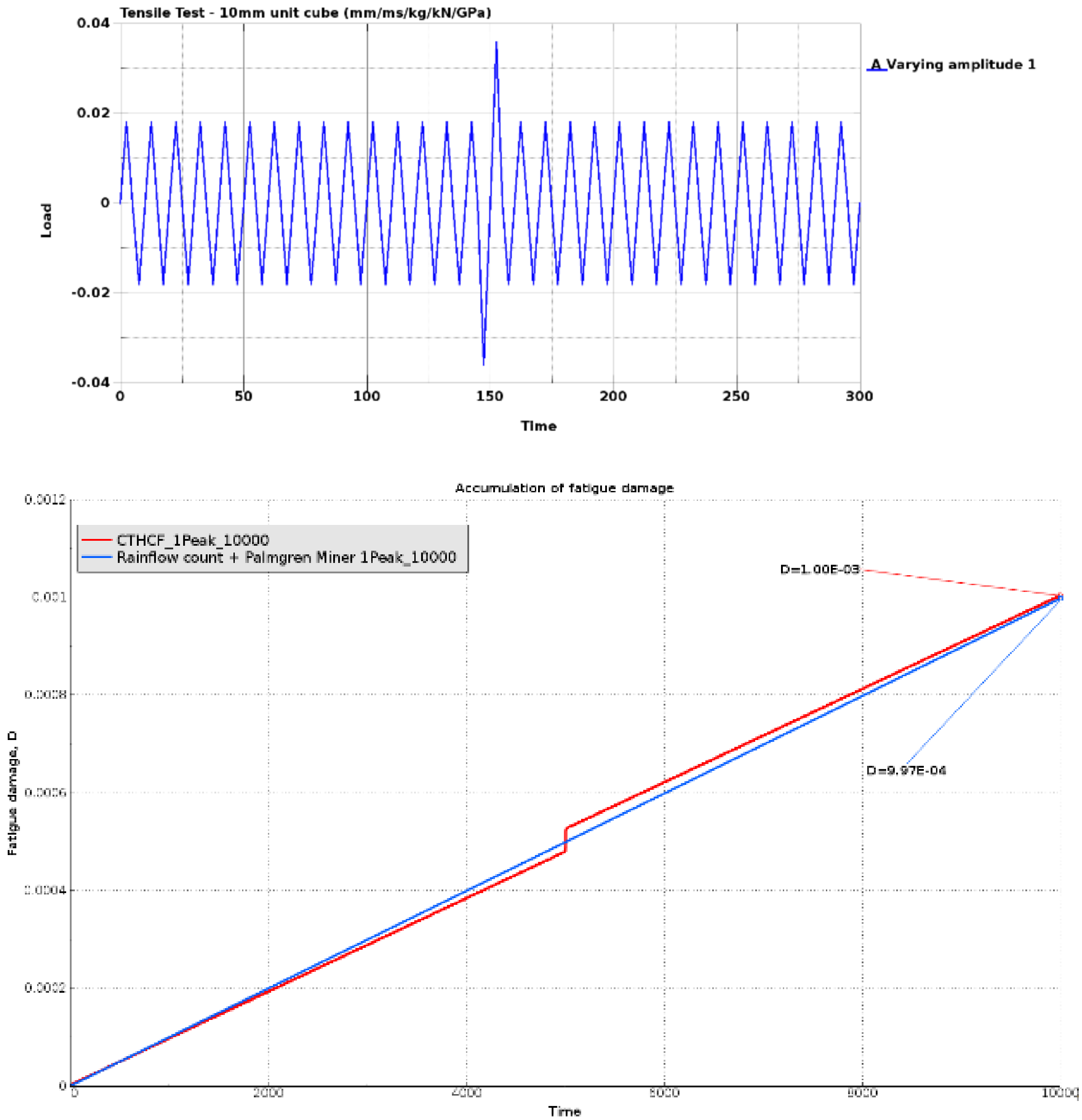

Figure 11. One peak amplitude in the spectrum, CTHCF compared to RFC+PM.

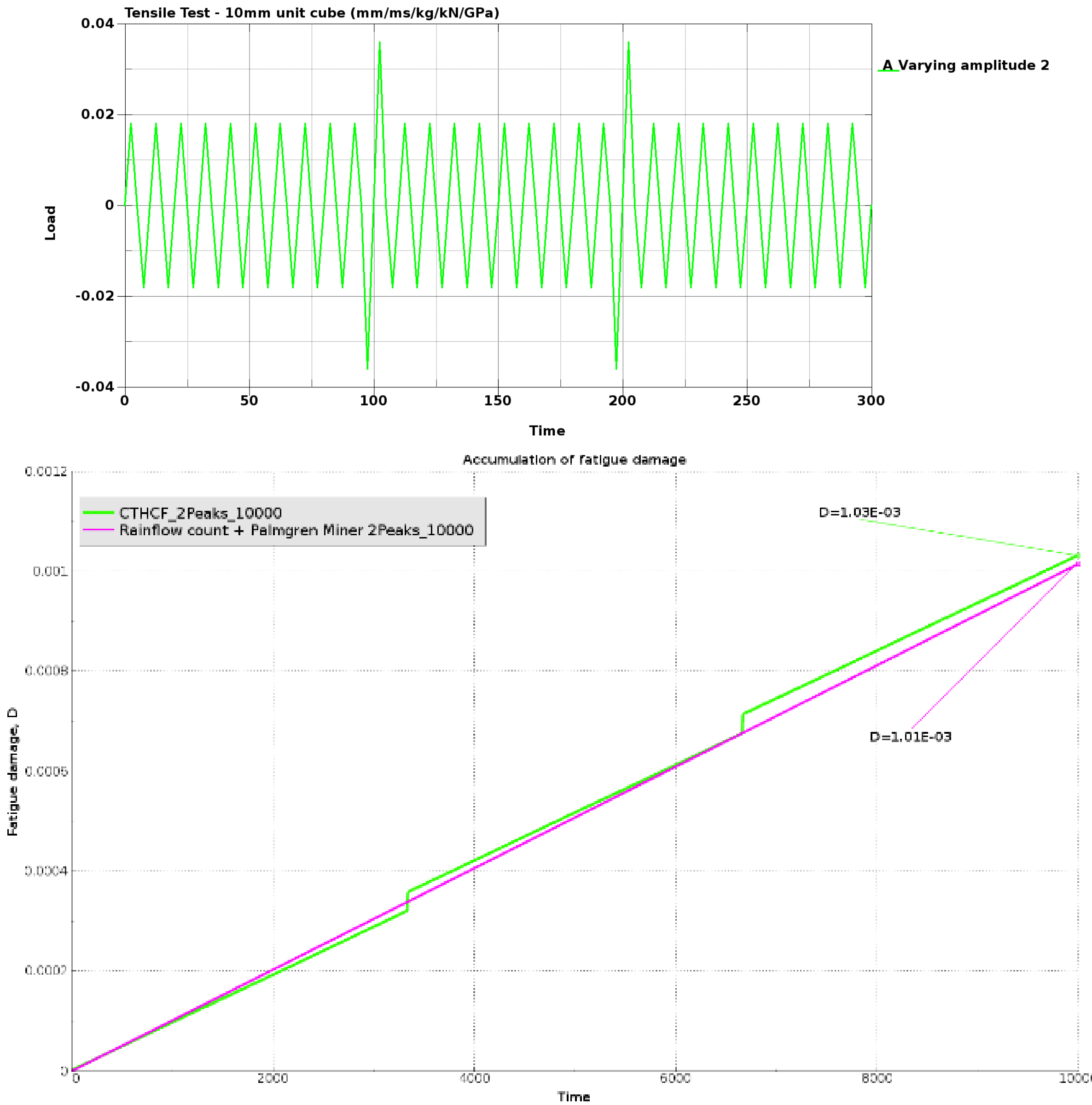

Figure 12. Two peak amplitudes in the spectrum, CTHCF compared to RFC+PM.

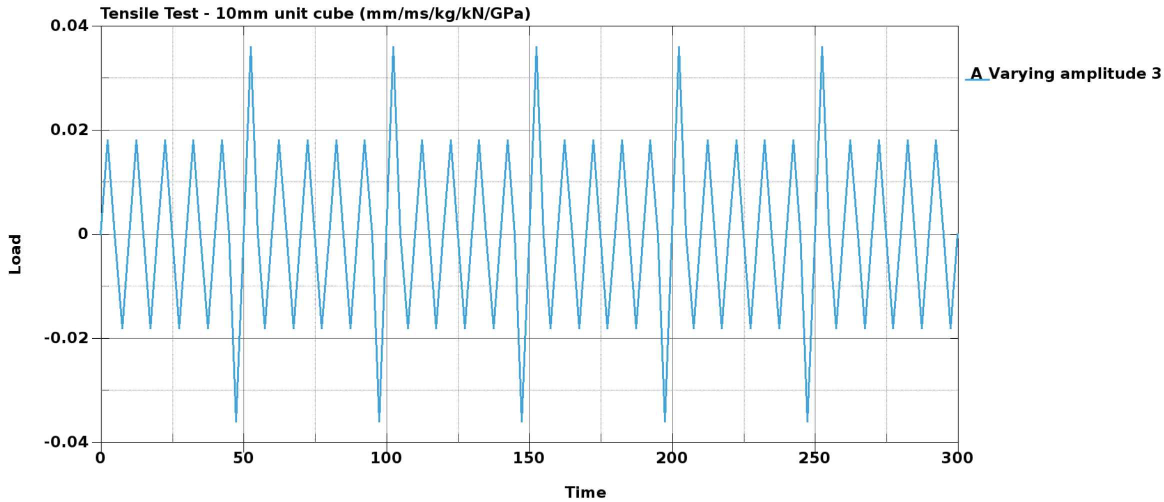

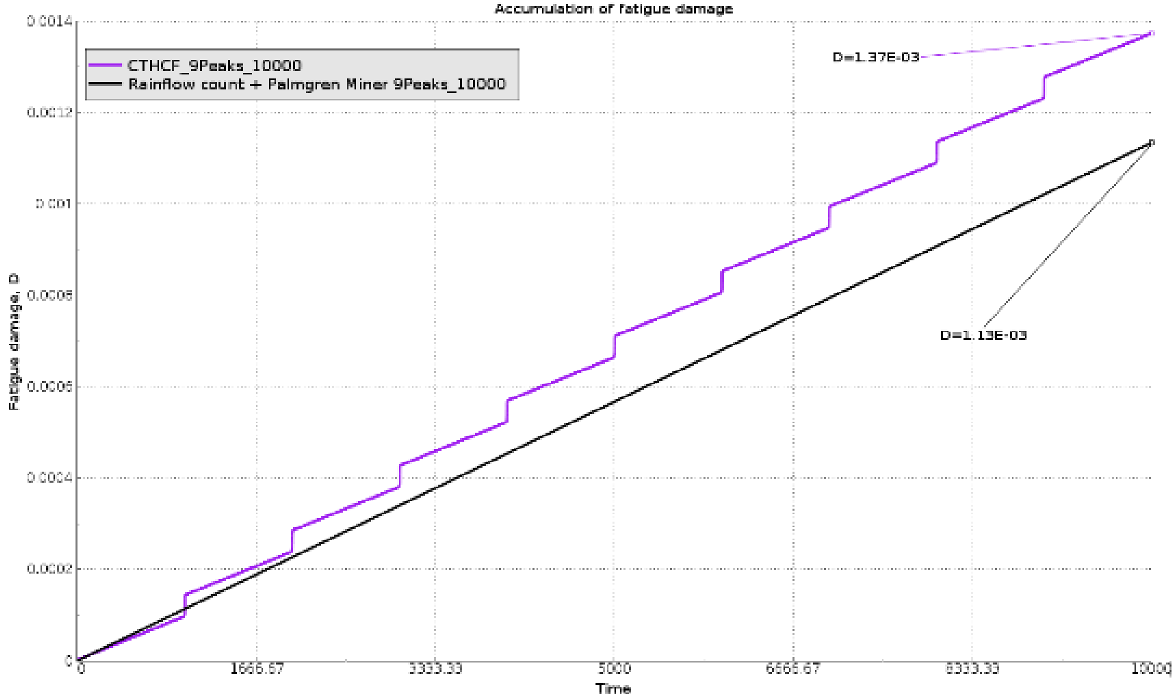

Figure 13. Nine peak amplitude in the spectrum, CTHCF compared to RFC+PM.

The difference was only 0.3% for the case with one peak load in the load spectra, cf. Figure 11, while it grew to about 2% for the case with two peaks load in the load spectra, cf. Figure 12. For the case with nine peaks, cf. Figure 13, the difference was about 17%. A comparison of the above evaluated load cases is summarised in Table 3.

Table 3. Results comparison for non-constant amplitude cases.

LOAD CASE	D, CTHCF	D, RFC+PM	DIFF [%]
CONSTANT AMPLITUDE	0.000980	0.000957	2
1 PEAK AMPLITUDE	0.001000	0.000997	0.3
2 PEAK AMPLITUDES	0.001010	0.001000	2
9 PEAK AMPLITUDES	0.001370	0.001300	17

Biaxial, non-proportional loading

Biaxial loading has also been studied, where one biaxial proportional load case and several biaxial and non-proportional load cases were studied and compared. The loads were applied according to Equations (6a) – (6c) The phase angles studied were 0°, 10°, 30°, 45°, 60° and 90°.

$$\sigma_{33} = \frac{\sigma_0}{\sqrt{2} \cdot \cos\left(\frac{\phi}{2}\right)} \cdot \sin(\omega t), \qquad (6a)$$

$$\sigma_{31} = \frac{\sigma_0}{\sqrt{6} \cdot \cos\left(\frac{\phi}{2}\right)} \cdot \sin(\omega t + \phi), \qquad (6b)$$

$$\sigma_{11} = \sigma_{22} = \sigma_{21} = \sigma_{32} = 0 \qquad (6c)$$

The phase dependence of the amplitudes in Eq. (6a) and (6b) ensures that the maximum stress reversal will result in the same amplitude independent of the phase-angle, ϕ. See Figure 14 for stress variations from combined axial and shear load (σ_0 =180 MPa).

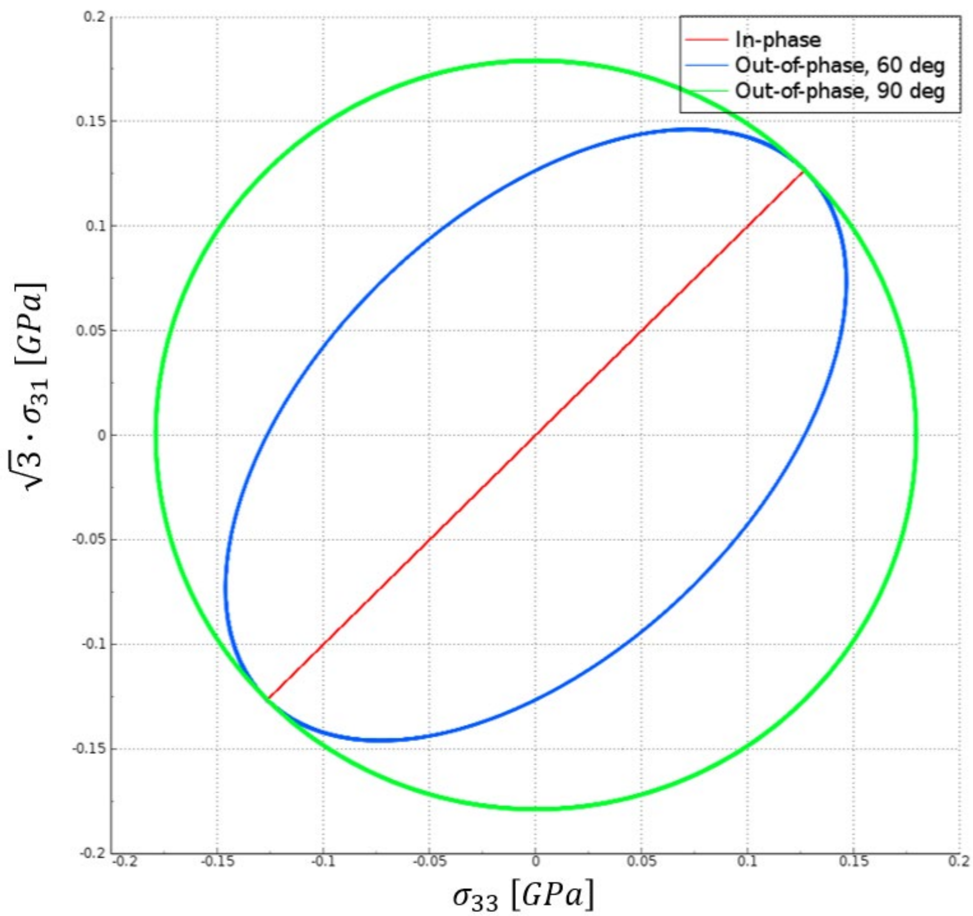

Figure 14. Element stress response for biaxial loading of the CTHCF-model.

The element stress response from biaxial loading are shown in Figure 15 below. The curves represent the axial stress(green), the shear stress(red) and the von Mises effective stress(blue), respectively.

$(\sigma_0 = 200\ MPa, \phi = 0°)$

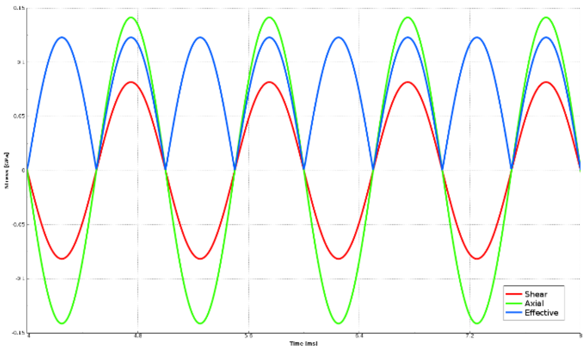

$(\sigma_0 = 200\ MPa, \phi = 10°)$

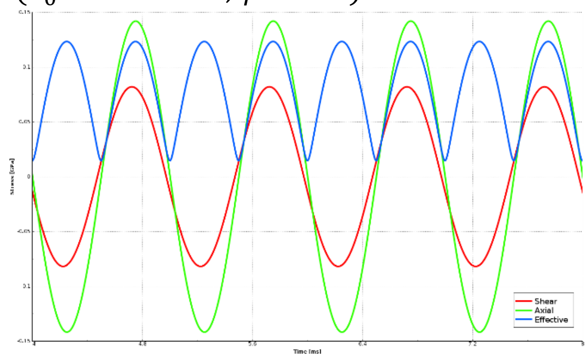

$(\sigma_0 = 200\ MPa, \phi = 30°)$

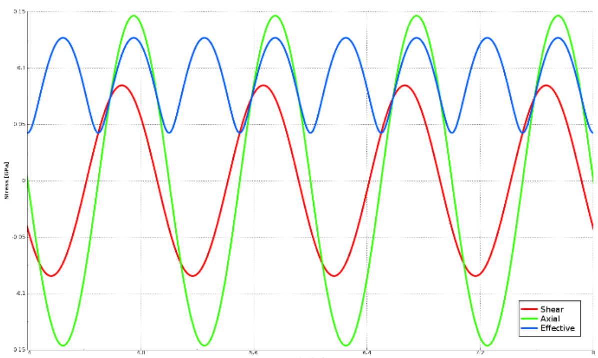

$(\sigma_0 = 200\ MPa, \phi = 45°)$

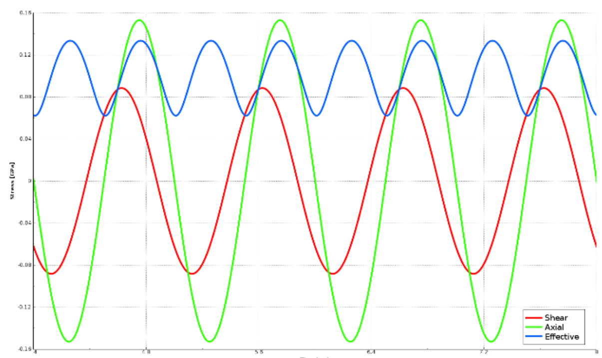

$(\sigma_0 = 200\ MPa, \phi = 60°)$

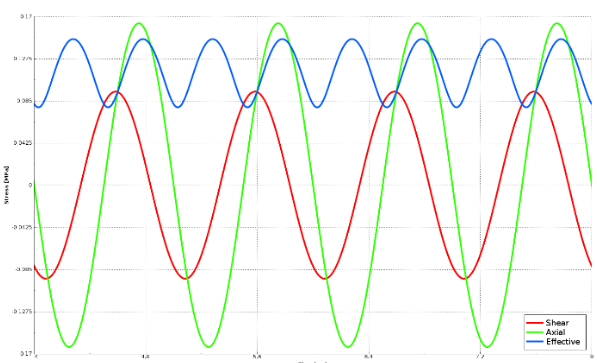

.$(\sigma_0 = 200\ MPa, \phi = 90°)$

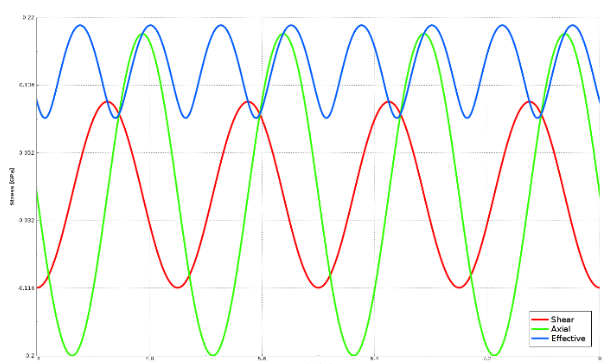

Figure 15. Biaxial, proportional and non-proportional loading scenarios.

When comparing fatigue damage evolution, it is seen that the model is not applicable for shear load with a phase angle that is more than 60 degrees out-of-phase as can be observed in Figure 16 and Figure 17.

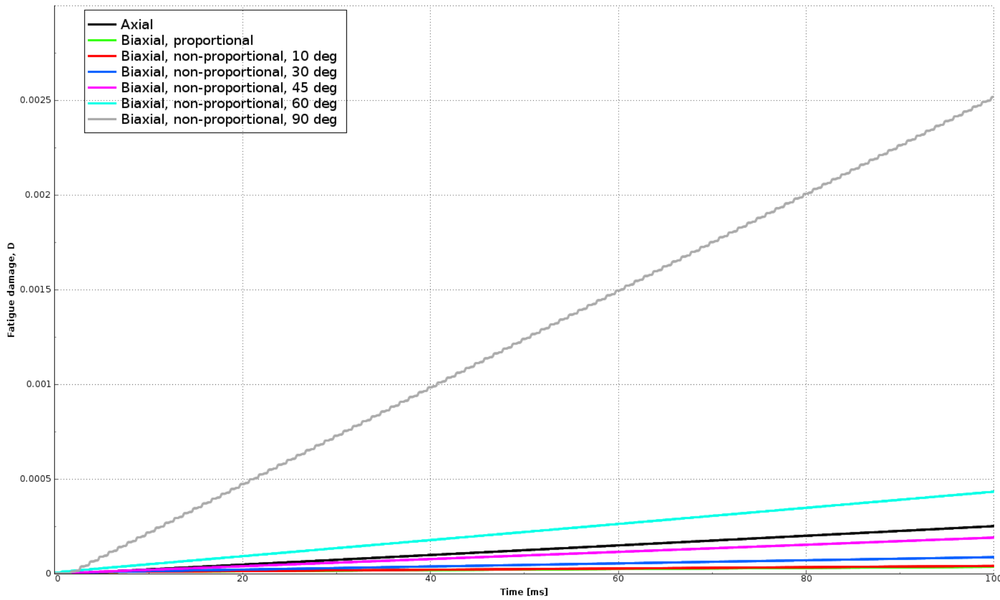

Figure 16. Biaxial, proportional and non-proportional loading.

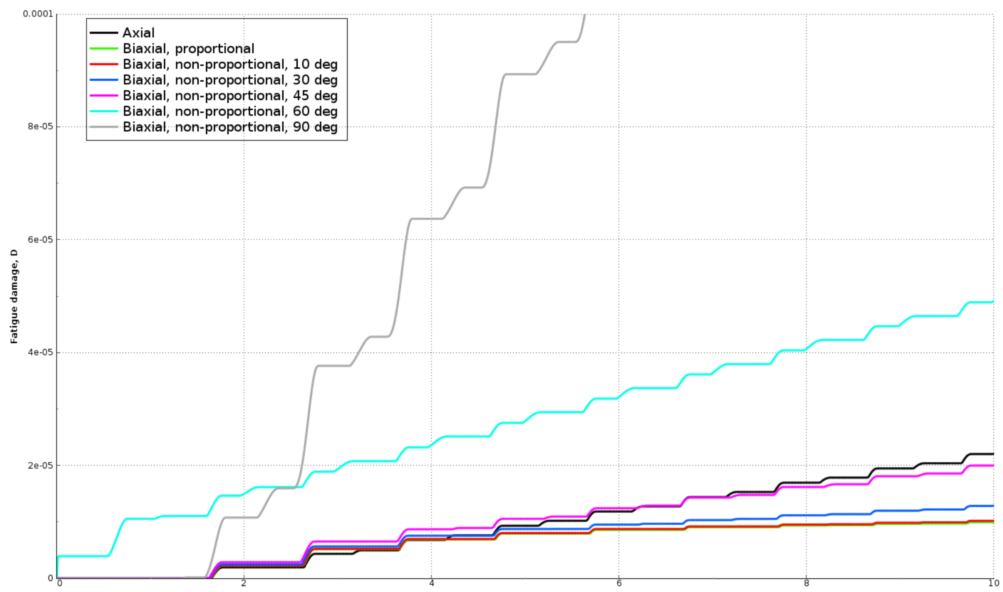

Figure 17. The CTHCF-model loses accuracy for non-proportional loading with phase angles about 60 degrees and more.

Tensile test comparison

A slightly larger model was studied in order to compare the damage at structural notches. The model and the results are shown in Figure 18.

Load case: Displacement controlled: $\Delta = A \cdot \sin(\omega t)$

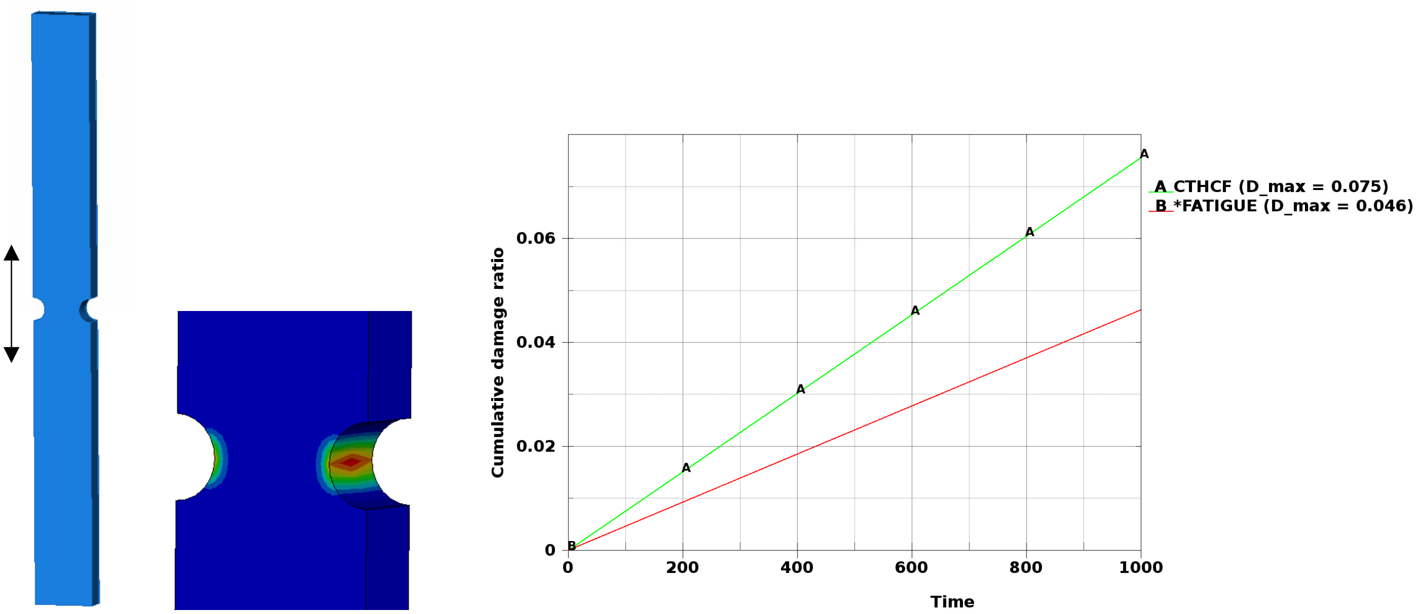

Figure 18. Test specimen and result.

Notch stresses are multiaxial by nature, which the CTHCF-model takes this into account by default. The results from mFAT, not presented here, are very close to the results from using *FATIGUE_MULTIAXIAL in LS-DYNA.

<u>Timing information:</u>
Nodes: 4375
Shells: 2384
Solids: 3072
Termination time: 1000
Number of cycles: 10000
Number of cores used: 2

Solution time without CTHCF-model(including *FATIGUE analysis): 1 h 18 min
Solution time with CTHCF: 1 h 39 min
Time penalty: 21 min (26%)

Conclusions and Further Work

The CTHCF-model shows a good agreement to test when considering uniaxial loads of constant amplitude. For uniaxial load spectrums with varying stress amplitudes the model deviates more from the traditional approach of rainflow count and Palmgren-Miner damage accumulation rule. The CTHCF-model yields a higher damage value in general.

For biaxial loading it was found that the CTHCF-model is not applicable when the shear load phase angle is about 60° or more.

The above issues have already been addressed and work is in progress for minimizing the deviation from the traditional method for varying amplitude loads and to also find a more accurate approach for non-proportional loading.

An important notice is that e.g. mFAT, and other common fatigue analysis tools are using the maximum principal stress at a critical plane to calculate the fatigue damage while the CTHCF-model is using the maximum shear stress in any plane so there should be a difference in the results. Also, due to the convergence behavior of the CTHCF-model the order of the load scenario will impact the end results while in classical fatigue theory the results are independent of the load order. What is more correct? Only testing can answer that.

Also, the simulation time penalty from using the CTHCF-model will be much less noticeable in a larger and more complex model such as the rock drill. This because other time-consuming features such as sensors, functions, advanced contacts, user-defined loadings, user defined material models, oil film damping, and other features are also included.

Acknowledgements

The contributions from SBL, DL and PS were funded by the National Aeronautical Research Program 7 of Vinnova as grant agreement No. 2019-02778.

References

[1] N. S. Ottosen, R. Stenström, and M. Ristinmaa. Continuum approach to high-cycle fatigue modeling. Int. J. Fatigue, 30(6):996–1006, 2008.
[2] S.B Lindström, S. Suresh, C.-J Thore, A. Klarbring. Continuous-time fatigue model: Acceleration for cyclic load. Int. Conf. on Material Modeling, Lund, 2019
[3] S.B Lindström, C.-J Thore, S. Suresh, A. Klarbring. Continuous-time, high-cycle fatigue model: Validity range and computational acceleration for cyclic stress. Int. J. Fatigue, 136:105582 (2020).
[4] S. Holopainen, R. Kouhia, T. Saksala. Continuum approach for modelling transversely isotropic high-cycle fatigue. Eur. J. Mech. A, 60:183–195 (2016).
[5] Jonsson, A., Sjöberg, M., and Grenwald, J., mFAT – a basic fatigue module for μETA – Post, 6th International BETA Conference, Thessaloniki 2015, internet source: https://www.beta-cae.com/events/c6pdf/4C_2_DYNAMORE.pdf
[6] Jonsson, A., mFAT v1.1 – fatigue analysis package for μETA, Dynamore Nordic Report 140411, Linköping 2015.
[7] META Post Processor version 20.0.X. User Guide, BETA CAE Systems International AG, 2019
[8] Livermore Software Technology, an ANSYS company, LS-DYNA Keyword User's Manual, 2020